13th U. S. National Combustion Meeting
Organized by the Central States Section of the Combustion Institute
March 19–22, 2023
College Station, Texas

# Single-camera Time-Resolved Laser-Induced Incandescence Measurements in a RQL Aeroengine Combustor

*Russell McGrath*[1], *Ezekiel M. Bugay*[1], *Jeremiah Juergensmeyer*[1], *Andy X. Zheng*[1], *David Wu*[1], *Adam Steinberg*[1], *Wenting Sun*[1], *Yi C. Mazumdar*[1,*]

[1] *Georgia Institute of Technology, North Avenue NW, Atlanta, GA, USA.*

[*] *Corresponding Author Email: ellen.mazumdar@gatech.edu*

**Abstract:** Understanding and measuring the formation of non-volatile particulate matter is important for minimizing emissions and improving the design of aeroengines. In rich-burn, quick-mix, lean-burn (RQL) combustors, significant quantities of soot are formed near the injectors, some of which is later oxidized downsteam. In order to better understand the soot formation dynamics in RQL burners, diagnostics that can measure both soot volume fraction and estimate soot particle sizes are needed. In this work, we describe the design, construction, and control of a high pressure RQL aeroengine combustor that is operated with Jet A fuel. Next, the development and implementation of two-dimensional single-camera time-resolved laser-induced incandescence (TiRe-LII) technique is described. In this technique, a single laser pulse is formed into a sheet and used to heat the soot inside the combustor. Then, a single ultra-high-speed camera is used to capture both the prompt LII signal and the soot incandescence decay over time at up to 10 MHz. By combining these images with a TiRe-LII model that is validated against soot sampling results from a Jet A flame, it is possible to estimate both the primary soot particle size and the soot volume fraction near the fuel injectors. By combining these measurements, a clearer picture of soot formation can be determined for RQL combustion.

***Keywords: Laser-induced Incandescence, Soot Volume Fraction, Soot Primary Particle Size, Rich-burn Quick-mix Lean-burn Combustor***

## 1. Introduction

Emissions of nvPM, which is composed primarily of soot, from aircraft engines can have detrimental impacts on human health [1] and the environment [2]. Presently, nvPM is considered the second most important human emission in terms of climate forcing [3]. The production of nvPM during combustion represents sub-optimal or poor combustion conditions, resulting in efficiency losses and increased potential for damage due to increased radiative heat transfer. The generation of nvPM in simple laminar flames of gaseous reactants or in homogeneous reactors has been extensively studied [4, 5, 6, 7]. However, the complicated thermodynamic and chemical processes involved in nvPM formation remain a challenge to accurately model even in simple systems. In aeronautical gas turbine combustors, the turbulent flow field, liquid fuel injection, and elevated-pressure operating conditions add new complications. Hence,

accurate prediction and control of nvPM in these environments represents a major challenge with significant practical consequences.

The production of solid carbonaceous nvPM involves inception, mass growth via surface chemical reactions or depositions, particle coagulation and mass loss by oxidation. The inception process begins with the formation of gas-phase precursors, of which PAH containing multiple rings are the most significant. The formation of the first PAH ring from small aliphatics is generally considered the rate limiting step in nvPM formation. The formation of larger PAH structures then follows, predominantly through the hydrogen abstraction carbon addition mechanism [8, 9] in which a hydrogen atom is abstracted from an aromatic molecule and replaced by an acetylene molecule. However, other mechanisms – such a ring-ring condensation – also may be significant if the concentration of aromatics is sufficiently high, which might be the case during poor mixing conditions in aeronautical gas turbine combustors. The subsequent mechanism that transitions the gas-phase species to nascent solid nvPM particles remains unclear, but likely involves the collision of large PAHs to form dimers, trimers, and so on. Nascent particles continue to grow through coalescence and/or addition of gas-phase species, eventually resulting in primary particles with a C-to-H ratio in the range of 10-20. These primary particles further agglomerate, forming chain-like aggregate structures with fractal characteristics. Important characteristics of the final nvPM structures include the primary particle size, aggregate properties, and primary particle number density.

Simultaneous and subsequent to the nvPM formation processes are chemical processes leading the nvPM oxidation, including conversion to CO and $CO_2$. It is the relative competition between formation and oxidation that ultimately determines the nvPM characteristics exiting the combustor. While other species may contribute to oxidation, collision with hydroxyl radicals (OH) and oxygen molecules ($O_2$) are the main oxidation pathways [5]. The relative importance of these pathways depends on the local composition, with OH-based oxidation being dominant in fuel-rich regions and $O_2$-based oxidation dominating in fuel-lean regions. Oxidation rates can be estimated through the product of a modelled collision rate and collision efficiency; though considerable uncertainty exists regarding efficiency values.

Owing to the complexity of nvPM formation kinetics, the majority of studies have been conducted in laminar flows (such as laminar diffusion jet flames [10], laminar premixed flames [11] and counterflow flames [12]) or homogeneous reactors such as shock tubes [13] to remove the complications due to turbulence, liquid fuel sprays, and temperature gradients. Most previously studied fuels were relatively simple gases, such as ethylene. With a few exceptions [12, 14], nvPM studies have also mostly been conducted at atmospheric pressure conditions. Studies of nvPM at real engine conditions, on the other hand, are largely missing from the literature. Specifically, the effects of spray pattern, turbulence, and mixing on nvPM formation and oxidation are poorly understood. Recent studies have begun unravelling some of these complexities. For example, recent work on a methane-fueled swirl flame in a gas turbine model combustor at atmospheric pressure showed how the persistent region of elevated OH in the central recirculation zone aided nvPM oxidation, effectively eliminating nvPM in the recirculation zone [15]. In contrast, a recent study in the same burner using liquid Jet-A fuel found nvPM mainly within the recirculation zone [2]. Such large-scale qualitative differences may arise due to differences in the fuel mixing rates, leading to nvPM formation occurring at different locations relative to the oxidizing OH.

Laser induced incandescence (LII) techniques are state-of-the-art methods for *in situ* characterization of nvPM volume fraction and primary particle size. However, most time-resolved LII (TiRe-LII) studies for estimating primary particle sizes are acquire at a single-point. While the measurement location can be traversed to build maps of soot particle size, the

lack of instantaneous spatial distributions places limitations on data interpretation, particularly in turbulent flames with transient combustion and mixing. In our recent work, we demonstrate two-dimensional soot particle size characterization using planar LII in turbulent jet flames at atmospheric pressure [16] and jet A fuels at elevated pressures [17, 18]. The single-camera single-laser-shot TiRe-LII technique can provide detailed information on the nvPM volume fraction by utilizing the prompt LII signal and primary particle size by fitting to the signal decay time constant across the image. These works were able to demonstrate varying particle size distributions in the soot growth regions versus the oxidation regions and demonstrated successful particle sizing in Jet A fuels.

In this paper, we report the first application of TiRe-LII in a high-pressure sector combustor employing liquid jet fuel for determining soot volume fraction and estimating soot particle size *in situ*. First, a time-resolved LII model is briefly described to show how the incandescence decay signals scale with different properties. Then, the construction of a pressurized rich-burn, quick-mix, lean-burn (RQL) combustor and LII diagnostic setup are outlined. Finally, preliminary results showing time-resolved LII data are described illustrating both the prompt LII signal, which is proportional to volume fraction, and the time-constant signal, which is proportional to primary soot particle size and the number of particles per soot aggregate. By analyzing the data obtained from this study, we can potentially understand the local instantaneous relationships between soot chemistry, combustion processes, and turbulent fluid dynamics.

## 2. Laser Induced Incandescence Model

To perform two-dimensional TiRe-LII, a high powered laser is formed into a sheet and passed through an area of interest. Soot particles that intersect the laser sheet absorb energy and heat up, causing them to incandesce. In order to capture the incandescence, a series of images are taken at high speed using filters to attenuate light from the laser as well as the $C_2$ Swan band emission while passing some of the gray body emission as the LII signal. The prompt and time-decay intensities of each pixel can be used to estimate soot volume fraction, particle sizes, and number of particles per aggregate. While time-decay fitting and calibration can be used, extracting quantitative particle sizing information from this data requires the use of a model that describes the heat and mass transfer effects on soot particles. One such model, developed by Liu [19], provides an energy conservation equation given by,

$$\frac{dU_{internal}}{dt} = \dot{Q}_{Absorption} - \dot{Q}_{Conduction} - \dot{Q}_{Radiation}, \tag{1}$$

where internal energy, absorption, and radiation are given by,

$$\frac{dU_{internal}}{dt} = \frac{\pi}{6} d^3 N_p \rho_s c_s \frac{dT}{dt}, \tag{2}$$

$$\dot{Q}_{Absorption} = \frac{\pi^2 d^3 E(m) F_0 q(t) N_p}{\lambda}, \tag{3}$$

$$\dot{Q}_{Radiation} = N_p \int_0^\infty \frac{8\pi^3 c^2 h}{\lambda^6} \frac{d^3 E(m)}{exp(hc/(k_B \lambda T)) - 1} d\lambda. \tag{4}$$

Here, $d$ is the primary particle size of the soot, $N_p$ is the number of particles per aggregate,

$\rho_s$ is the density of soot, $c_s$ is the specific heat of soot, $E(m)$ is the refractive index function, $F_0$ is laser fluence, $q(t)$ is laser temporal profile function, $\lambda$ is laser wavelength, and $T$ is temperature. The fundamental constants are $h$ for the Planck constant, $k_b$ for the Boltzmann constant, and $c$ for the speed of light.

At low laser fluences, sublimation can be ignored and conduction is the most dominant form of heat transfer, playing a large role in the decay time of the incandescence. Here, we model conduction using Fuchs method [20, 21, 22] where the conduction is split between a free-molecular regime near the particle and the continuum regime further away from the particle. Conduction in the free-molecular regime near the soot particle can be modeled as,

$$\dot{Q}_{Conduction} = \alpha \pi R_a^2 \frac{p_g}{2} \sqrt{\frac{8 k_B T_\delta}{\pi m_g}} \frac{\gamma^* + 1}{\gamma^* - 1} \left( \frac{T}{T_\delta} - 1 \right), \tag{5}$$

where $p_g$ is the pressure, $m_g$ is the mass of a gas molecule, $T_\delta$ is the temperature at the limiting sphere between the two regimes, $\alpha$ is the thermal accommodation coefficient for soot, and $R_a$ is the equivalent sphere radius calculated based on the aggregate projected area. Here, $\gamma^*$ is the average specific heat ratio given by,

$$\frac{1}{\gamma^* - 1} = \frac{1}{T - T_\delta} \int_{T_\delta}^{T} \frac{1}{\gamma - 1} dT. \tag{6}$$

In the continuum regime, conduction an be modeled using,

$$\dot{Q}_{Conduction} = 4\pi(\delta + R_a) \int_{T_g}^{T_\delta} k_g dT, \tag{7}$$

where $\delta$ is the limiting sphere boundary layer thickness used in the Fuchs method and $k_g$ is the thermal conductivity of the gas. By solving this set of equations, it is possible to estimate the temperature of a soot particle as a function of time. By converting temperatures to a signal proportional to light emission using the Planck equation, it is possible to compare theoretical and experimental intensities.

Using this modeling technique, the intensity of the emitted signal in each pixel immediately after laser pulse arrival can be approximated as roughly proportional to the soot volume fraction. The incandescence decay time constant, however, is influenced by the soot primary particle size, number of particles per aggregate, ambient pressure, ambient temperature and other factors. By estimating or measuring some these parameters, it is then possible to create a relationship between the incandescence decay time and the primary particle size.

## 3. Rich-burn Quick-mix Lean-burn Combustor Design

A rich-burn, quick-mix, lean-burn combustors were first introduced in 1980 [23] as a concept to reduce NOx emissions in gas turbine engines. The main characteristics of the RQL combustor are a primary stage with a rich equivalence ratio, followed by an air jet section that quenches the reaction, leading to the secondary state with a lean equivalence ratio [24]. The RQL combustor in this work is a custom article designed at Georgia Tech. The combustor system is composed of a pressure chamber with optical access, a fuel subsystem, an air subsystem, a triple-injector optical liner subsystem, a water-cooled exhaust, and a hydrogen ignitor. Figure 1a illustrates a schematic of the pressure chamber and supporting fuel and air subsystems. The optically accessible pressure chamber is stainless-steel and has a 46 cm

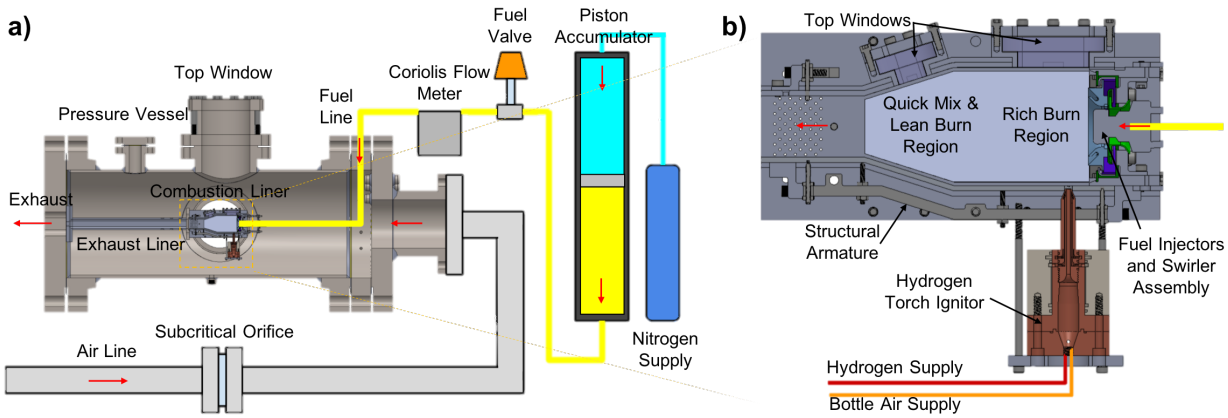


Figure 1: a) The major components of the pressurized combustor include the pressure vessel, air line components, fuel line components, combustion liner assembly, and exhaust liner. b) A magnified view of the combustion liner assembly show the fuel inectors and swirlers, the fuzed quartz windows, the structural armature, the hydrogen torch ignitor, the rich burn region, and the quick-mix lean-burn region.

inner diameter with a pressure rating of 31 bar and temperature rating of 510 °C. Each of the pressure chamber's three windows (one top and two sides) are 10 inches in diameter and made of fused quartz. To control fuel flow, nitrogen is used to pressurize a Parker piston accumulator [25], which depresses a piston to drive Jet A fuel into a control valve and a Bronkhorst Coriolis flow meter [26]. The Jet A fuel is then sent through a squeeze flange in the pressure chamber and into an insulated manifold that mates with the triple-injector liner. High temperature air is supplied to the pressure chamber via a preheated air-supply, which can provide variable static pressure (up to 50 bar) and temperature (up to 1100 K).

The side-view of the triple-injector optical liner subsystem is detailed in Fig. 1b. The liner article is a modular unit with discrete top, bottom, and side sections, supported by a skeletal frame armature. To reduce machining time and cost, the top and bottom plates with angled effusion cooling holes were 3D-printed in Inconel 718. The top plate features two fused-quartz windows that are used for visualization by the high-speed camera system, while the side plates feature a single fused quartz window on each side for passing collimated laser beams and for optical monitoring. As previously mentioned, the fuel manifold from inside the pressure chamber mates to the liner. This is done through the insertion of three aircraft fuel injectors provided by Honeywell, which spray into corresponding fuel swirlers. The general layout of this liner was chosen to emulate a small section of an annular combustion liner commonly found in aircraft engines. By testing the interaction between multiple fuel swirlers, it is possible to observe the interactions between the fuel sprays and flow fields which drive nvPM formation. The triple-injector optical liner is then attached to a custom water-cooled exhaust section, which is rigidly attached to the rear flange of the pressure chamber. To initiate combustion inside the chamber, a hydrogen torch ignitor with a small glow plug is used. Here, a premixed hydrogen and air flame is first ignited, which is followed by a diffusion flame. This, in turn, ignites the rich Jet A fuel mixture as it enters the liner. Each of the RQL combustor's subsystems are controlled individually in an adjacent control room. A custom LabView program is used to monitor and adjust the subsystems in real time, while an additional computer is used for gathering diagnostic data from the LII camera, laser controllers, timing boxes, and laser power meters.

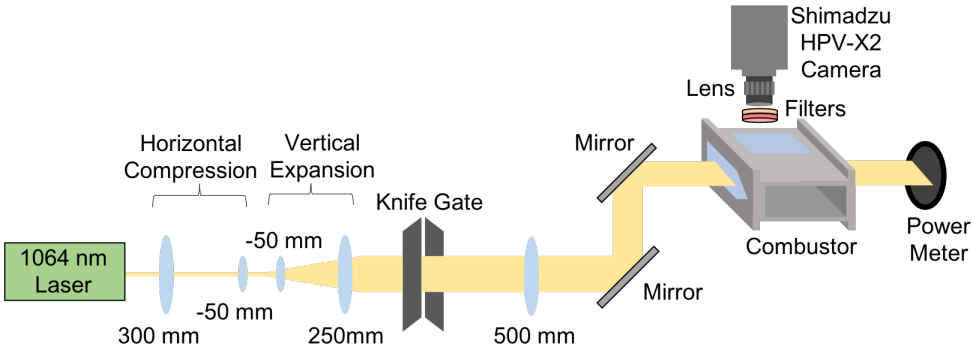


Figure 2: The optical setup for time-resolved LII is shown with the 1064 nm laser, lenses, knife gate, mirrors, combustor, filters, camera, and power meter.

## 4. Single-Camera Time-Resolved Laser Induced Incandescence Setup

Single-camera single-laser-shot time-resolved laser induced incandescence is an optical diagnostic technique where a high-powered laser sheet is used to rapidly heat soot particles, causing them to incandesce. This incandescence decay is then captured by a high speed camera using through a series of filters. To determine the soot volume fraction, a power meter is used to measure the energy loss of the laser across the flame section. By comparing the prompt LII signal from the high speed camera with the energy lost across the flame the volume fraction of soot can be estimated. To determine soot particle size or number of particles per soot aggregate, the the decay time of the LII signal in each pixel is fit to a validated LII model as described in Section 2.

To heat the soot, an Nd:YAG laser (Spectra-Physics Quanta-Ray Pro-250) was used to generate a 1064 nm laser beam with a diameter of approximately 10 mm. Then, a series of cylindrical lenses were used to horizontally compress (300 mm and -50 mm lenses) and vertically expand (-50 mm and 250 mm lenses) the beam to a dimension of approximately 2 mm wide by 50 mm tall, as illustrate in Fig. 2. The laser sheet was then passed through a knife gate to create a tophat profile. This beam is then relay imaged into the center of the combustor using a cylindrical lens with a focal length of 500 mm. To capture the soot generation across all three injectors, the beam is aligned horizontally through the pressure vessel windows.

The image was then captured using a high speed camera (Shimadzu HPV-X2, 10-bit, 32 $\mu$m pixel size) with a 35 or 100 mm lens. To prevent unwanted reflections and to reject $C_2$ Swan band emissions, at 1064 nm bandstop filter and a 640 nm bandpass filter (75 nm full width at half maximum) were added. Data was collected at a framerate of 10 MHz (55 ns exposure, 250 $\times$ 400 pixels with zig-zag interpollation), allowing for capture of both the prompt LII signal for volume fraction estimation and time decay signal at lower pressures for soot particle sizing. To coordinate the timing of the laser pulse and camera capture, a timing box is used. Timing is closely monitored by using an oscilloscope connected to the camera as well as a photodiode directed at scattered light from the beam. At the same time, the power of the transmitted beam was also monitored using an energy meter.

## 5. Experimental Results

Initial experiments conducted in the facility with a vessel air temperature of 530 K and a vessel pressure of 64 psi. Once the vessel was preheated and the desired pressure and tem-

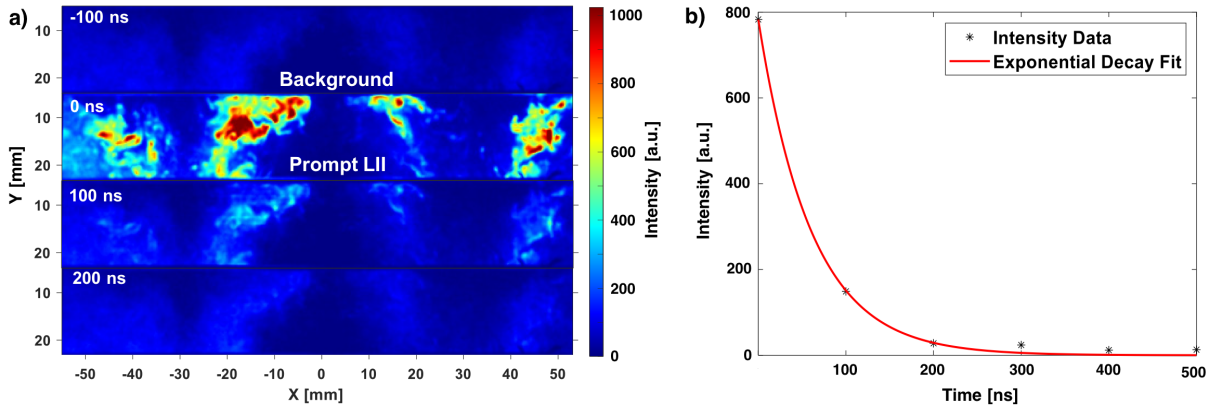


Figure 3: a) The time-resolved LII images are collected at 10 MHz showing the background image, the prompt LII signal (proportional to soot volume fraction) and signal decay. The $x$ dimension is the distance from the combustor centerline and $y$ is distance from the combustor dome face. The flames from the center swirl injector, half of the flow from the left injector, and half of the flow from the right injectors are visible. Flow in this image advances from the top of each sub-image to the bottom of each sub image. b) The signal from each pixel is fit to the LII model to determine decay time constants.

perature conditions were reached, the ignitor was initiated and a stable flame was achieved across the three injectors and swirlers. At the same time, the time-resolved LII data is collected using the high speed camera and power meter. Fig. 3a shows the decay of an LII signal over several frames with the laser operating at a fluence of 0.12 $J/cm^2$. These images were captured from approximately 5 mm to 23 mm downstream of the dome face with the laser beam passing through the center of the injectors. The middle injector can be seen centered in the image while parts of the flame from the left and the right injectors can also be seen.

Immediately before the arrival of the laser pulse, the high speed camera captures the line-of-sight background luminescence of the sooty flame in the rich-burn region. Due to the fast frame rate of the camera, the background luminescence does not change between flames. At $t = 0ns$, the laser pulse arrives and the bright prompt LII signal can be imaged. Due to the large field of view and high efficiency of the camera pixels, no intensifier is needed. This prompt LII signal, which is roughly proportional to the volume fraction, shows several regions with higher soot volume fractions as well as several turbulent flame features. In the following frames, the incandescence at each pixel decays over time until it is indistinguishable from the background. Figure 3b shows the LII signal fit to an exponential decay model, which matches well with the experimental data. This can then be used to determine time constant of thermal decay on a per-pixel basis.

Figure 4 shows a plot of the fitted time constants for every pixel in the image. Here, pixels with low intensities or high fitting uncertainties were set to black. One of the interesting features to note is that the pattern in the prompt LII signal is not heavily correlated with the time-constant image. This shows that the volume fraction is not heavily correlated with the primary soot particle size or number of particles per aggregate. In general, slightly higher intensity values were recorded upstream in the prompt signal, visible in Fig. 3a, while slightly higher time constants are present downstream. This may indicate a higher volume fraction

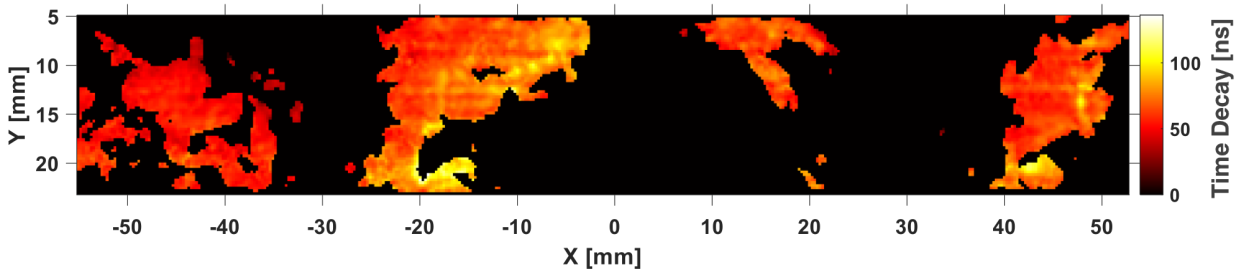


Figure 4: The fitted time constants for each pixel are plotted to show a signal proportional to the primary soot particle size and soot aggregate number. Pixels with low intensities or high fitting uncertainties were set to black. The $x$ dimension is the distance from the combustor centerline and $y$ is distance from the combustor dome face.

of soot upstream, while the growth of soot particles or agglomeration of particles creates higher local time constants downstream. Additional data at different operating conditions is needed to determine possible trends.

## 6. Conclusions

In this work, we demonstrate the application of a single-camera time-resolved laser-induced incandescence technique in a RQL aeroengine combustor. The high pressure combustor is described along with LII model trends and the optical setup. Initial results are promising, showing a strong incandescence signal with moderate laser fluences. Additionally, despite the high operating pressure inside the vessel, it was possible to fit time-decay constants to the incandescence data. This can potentially enable the determination of soot particle sizes or the average number of agglomerates per soot aggregate at elevated pressue conditions.

Potential future work includes expanding the field of view to examine the full rich burn region as well as part of the quick mix and lean burn regions, validating the LII measurements for volume fraction estimation and soot particle sizing, and examining combustion processes with OH planar laser induced fluorescence. By applying the techniques discussed in this paper, it is possible to study combustion trends at different operating conditions for an RQL aeroengine combustor at elevated pressures. This can help us gain a deeper understanding of local instantaneous relationships between turbulence, soot chemistry, and other combustion processes. The information can then be used to help design systems that reduce soot production while also maximizing combustor efficiency and performance.

## 7. Acknowledgements

The authors would like to thank Fang Xu, Rudy Dudebout, and Dustin Brandt at Honeywell International Inc. for their collaboration on this project and assistance with combustor design. This research was funded by the U.S. Federal Aviation Administration Office of Environment and Energy through ASCENT, the FAA Center of Excellence for Alternative Jet Fuels and the Environment, Project 70 through FAA Award Number 13-C-AJFE-GIT-080 under the supervision of Prem Lobo. Any opinions, findings, conclusions or recommendations expressed in this material are those of the authors and do not necessarily reflect the views of the FAA.

## 8. References


[1] J. S. Lighty, J. M. Veranth, and A. F. Sarofim, "Combustion aerosols: factors governing their size and composition and implications to human health," *Journal of the Air & Waste Management Association*, vol. 50, no. 9, pp. 1565–1618, 2000.

[2] L. Wang, C. K. Bauer, and O. L. Gülder, "Soot and flow field in turbulent swirl-stabilized spray flames of jet A-1 in a model combustor," *Proceedings of the Combustion Institute*, vol. 37, no. 4, pp. 5437–5444, 2019.

[3] T. C. Bond, S. J. Doherty, D. W. Fahey, P. M. Forster, T. Berntsen, B. J. DeAngelo, M. G. Flanner, S. Ghan, B. Kärcher, D. Koch, S. Kinne, Y. Kondo, P. K. Quinn, M. C. Sarofim, M. G. Schultz, M. Schulz, C. Venkataraman, H. Zhang, S. Zhang, N. Bellouin, S. K. Guttikunda, P. K. Hopke, M. Z. Jacobson, J. W. Kaiser, Z. Klimont, U. Lohmann, J. P. Schwarz, D. Shindell, T. Storelvmo, S. G. Warren, and C. S. Zender, "Bounding the role of black carbon in the climate system: A scientific assessment," *Journal of Geophysical Research: Atmospheres*, vol. 118, pp. 5380–5552, 2013.

[4] B. S. Haynes and H. G. Wagner, "Soot formation," *Progress in Energy and Combustion Science*, vol. 7, pp. 229–273, 1981.

[5] M. Frenklach and H. Wang, "Detailed modeling of soot particle nucleation and growth," *International Symposium on Combustion*, vol. 23, no. 1, pp. 1559–1566, 1990.

[6] H. Wang, "Formation of nascent soot and other condensed-phase materials in flames," *Proceedings of the Combustion Institute*, vol. 33, no. 1, pp. 41–67, 2011.

[7] A. E. Karatas and L. Gülder, "Soot formation in high pressure laminar diffusion flames," *Progress in Energy and Combustion Science*, vol. 38, pp. 818–845, 2012.

[8] M. Frenklach and H. Wang, "Detailed modeling of soot particle nucleation and growth," in *Symposium (International) on Combustion*, vol. 23, no. 1, 1991, pp. 1559–1566.

[9] M. Frenklach, "Reaction mechanism of soot formation in flames," *Physical Chemistry Chemical Physics*, vol. 4, no. 11, pp. 2028–2037, 2002.

[10] B. Franzelli, M. Roussillo, P. Scouflaire, J. Bonnety, R. Jalain, T. Dormieux, S. Candel, and G. Legros, "Multi-diagnostic soot measurements in a laminar diffusion flame to assess the ISF database consistency," *Proceedings of the Combustion Institute*, vol. 37, no. 2, pp. 1355–1363, 2019.

[11] P. Desgroux, A. Faccinetto, X. Mercier, T. Mouton, D. A. Karkar, and A. E. Bakali, "Comparative study of the soot formation process in a 'nucleation' and a 'sooting' low pressure premixed methane flame," *Combustion and Flame*, vol. 184, pp. 153–166, 2017.

[12] K. Gleason, F. Carbone, and A. Gomez, "Pressure and temperature dependence of soot in highly controlled counterflow ethylene diffusion flames," *Proceedings of the Combustion Institute*, vol. 37, no. 2, pp. 2057–2064, 2019.

[13] H. Wang, *Particulate Formation and Analysis*. Academic Press, 2001, vol. 3.

[14] K. P. Geigle, J. Zerbs, R. Hadef, and C. Guin, "Laser-induced incandescence for soot measurements in an aero-engine combustor at pressures up to 20 bar," *Applied Physics B*, vol. 125, no. 6, p. 96, may 2019.

[15] L. Wang, S. Chatterjee, Q. An, A. M. Steinberg, and L. Gülder, "Soot formation and flame structure in swirl-stabilized turbulent non-premixed methane combustion," *Combustion and Flame*, vol. 209, pp. 303–312, 2019.

[16] Y. Chen, E. Cenker, D. R. Richardson, S. P. Kearney, B. R. Halls, S. A. Skeen, C. R. Shaddix, and D. R. Guildenbecher, "Single-camera, single-shot, time-resolved laser-induced incandescence decay imaging," *Optics Letters*, vol. 43, no. 21, 2018.

[17] A. X. Zheng, S. R. Manikandan, S. E. Wonfor, A. M. Steinberg, and Y. C. Mazumdar, "Planar time-resolved laser-induced incandescence for particulate emissions in premixed flames at elevated pressures," in *AIAA SciTech Forum*, 2023.

[18] M. L. Passarelli, S. E. Wonfor, A. X. Zheng, S. R. Manikandan, Y. Mazumdar, J. M. Seitzman, A. M. Steinberg, H. Bower, J. Hong, K. Venkatesan, and M. Benjamin, "Experimental characterization of a lean pre-vaporized premixed combustor for supersonic transport applications," in *AIAA SciTech Forum*, 2022.

[19] F. Liu, G. J. Smallwood, and D. R. Snelling, "Effects of primary particle diameter and aggregate size distribution on the temperature of soot particles heated by pulsed lasers," *Journal of Quantitative Spectroscopy and Radiative Transfer*, vol. 93, no. 1-3 SPEC. ISS., 2005.

[20] A. V. Filippov and D. E. Rosner, "Energy transfer between an aerosol particle and gas at high temperature ratios in the Knudsen transition regime," *International Journal of Heat and Mass Transfer*, vol. 43, no. 1, 2000.

[21] N. A. Fuchs, "On the stationary charge distribution on aerosol particles in a bipolar ionic atmosphere," *Pure and Applied Geophysics*, vol. 56, no. 1, p. 185, 1963.

[22] N. A. Fuchs, R. E. Daisley, M. Fuchs, C. N. Davies, and M. E. Straumanis, "The mechanics of aerosols," *Physics Today*, vol. 18, no. 4, p. 73, 1965.

[23] S. A. Mosier and R. M. Pierce, "Advanced combustion systems for stationary gas turbine engines: Volume I. review and preliminary evaluation," U.S. Environmental Protection Agency Interagency Energy/Environment RD Program Report, EPA-600/7-80-017a, 1980.

[24] S. Samuelsen, *The Gas Turbine Handbook*. Morgantown, WV, USA: U.S. Department of Energy, 2006, ch. 3.2.1.3 Rich Burn, Quick-Mix, Lean Burn (RQL) Combustor.

[25] Parker Hannifin, "Piston accumulators." [Online]. Available: https://www.parker.com/literature/Global%20Accumulator%20Division/Catalogs%20&%20Bulletins/GAD%20HY10-1630%205-2012/HY10_1630US_5_2012-Piston_Accumulators.pdf.

[26] Bronkhorst, "Cori-flow coriolis mass flow meters/controllers for liquids and gasses." [Online]. Available: https://www.bronkhorst.com/getmedia/cc5bcd32-c21f-4984-85c9-7bc8fbfa2e65/CORI-FLOW-960032.pdf

# Technical Report Documentation Page

| 1. Report No. | 2. Government Accession No. | 3. Recipient's Catalog No. |
|---|---|---|
| McGrath_TiReLII_USNCM2023 | | |

| 4. Title and Subtitle | 5. Report Date |
|---|---|
| Single-camera Time-Resolved Laser-Induced Incandescence Measurements in a RQL Aeroengine Combustor | March 2023 |
| | 6. Performing Organization Code |

| 7. Author(s) | 8. Performing Organization Report No. |
|---|---|
| Russell McGrath, Ezekiel M. Bugay, Jeremiah Juergensmeyer, Andy X. Zheng, David Wu, Adam Steinberg, Wenting Sun, Yi C. Mazumdar | |

| 9. Performing Organization Name and Address | 10. Work Unit No. (TRAIS) |
|---|---|
| Center of Excellence for: Alternative Jet Fuels and Environment<br><br>Georgia Institute of Technology, Atlanta, GA, USA. | 11. Contract or Grant No.<br><br>13-C-AJFE-GIT-080 |

| 12. Sponsoring Agency Name and Address | 13. Type of Report and Period Covered |
|---|---|
| Federal Aviation Administration<br>Office of Environment and Energy | Conference Proceedings |
| | 14. Sponsoring Agency Code |

15. Supplementary Notes

https://sites.gatech.edu/chen-mazumdar/files/2026/02/McGrath_TiReLII_USNCM2023.pdf

16. Abstract

Understanding and measuring the formation of non-volatile particulate matter is important for minimizing emissions and improving the design of aeroengines. In rich-burn, quick-mix, lean-burn (RQL) combustors, significant quantities of soot are formed near the injectors, some of which is later oxidized downsteam. In order to better understand the soot formation dynamics in RQL burners, diagnostics that can measure both soot volume fraction and estimate soot particle sizes are needed. In this work, we describe the design, construction, and control of a high pressure RQL aeroengine combustor that is operated with Jet A fuel. Next, the development and implementation of two-dimensional single-camera time-resolved laser-induced incandescence (TiRe-LII) technique is described. In this technique, a single laser pulse is formed into a sheet and used to heat the soot inside the combustor. Then, a single ultra-high-speed camera is used to capture both the prompt LII signal and the soot incandescence decay over time at up to 10 MHz. By combining these images with a TiRe-LII model that is validated against soot sampling results from a Jet A flame, it is possible to estimate both the primary soot particle size and the soot volume fraction near the fuel injectors. By combining these measurements, a clearer picture of soot formation can be determined for RQL combustion.

| 17. Key Words | 18. Distribution Statement |
|---|---|
| Laser-induced Incandescence, Soot Volume Fraction, Soot Primary Particle Size, Rich-burn Quick-mix Lean-burn Combustor, ASCENT | |

| 19. Security Classif. (of this report) | 20. Security Classif. (of this page) | 21. No. of Pages | 22. Price |
|---|---|---|---|
| Unclassified | Unclassified | | |